Long-time dynamics of the three-dimensional biaxial Grinfeld instability

Jérôme Paret*

Laboratoire Matériaux et Microélectronique de Provence, CNRS UMR 6137, Faculté des Sciences de St Jérôme, case 142, 13397 Marseille cedex 20, France

(Received 30 July 2004; revised manuscript received 10 December 2004; published 15 July 2005)

Using a phase-field model including strain fields, we numerically investigate the melting-crystallization dynamics of a biaxially stressed semi-infinite solid. A multigrid algorithm is used to solve the elasticity part of the problem. Its efficiency allows us to explore the late stages of the full 3D Grinfeld instability. Recent analytical predictions [P. Berger *et al.*, Phys. Rev. Lett. **90**, 176103 (2003)] regarding stability and selection of patterns are confirmed and precised. It appears that, in the presence of a large scale stabilization mechanism, the system reaches an equilibrium state corresponding to a nontrivial striped pattern.

DOI: 10.1103/PhysRevE.72.011105 PACS number(s): 81.10.Aj, 05.70.Ln, 62.20.−x, 68.35.Md

In a recent paper [1], Berger *et al.* have analyzed the morphological stability of the surface of a semi-infinite solid submitted to a biaxial stress during a melting-crystallization process. Like in the original Asaro-Tiller-Grinfeld case for uniaxially stressed solids [2,3], a corrugated surface has lower elastic energy and, without a large scale stabilization mechanism such as gravity, any long-wavelength perturbation of an initially planar surface is amplified. However, contrary to the uniaxial case which yields one or several parallel deep grooves as a result of the instability, the biaxially stressed surface can evolve into nontrivial patterns. Indeed, it is shown in [1] that there exists a range of applied stresses where two systems of tilted stripes may coexist to form a diamond pattern. Analytical predictions about physical problems involving elasticity and/or pattern selection being notoriously difficult, their result marks a new step in the understanding of the general problem of interfacial dynamics driven by elastic stresses. This is also of practical importance since this elasticity-driven instability is known to be the cause of the decomposition via surface diffusion of epitaxially grown thin films into islands (Stranski-Krastanov island-on-layer growth mode) [4]. Diamond patterns could thus constitute a pathway to self-organized quantum dots arrays. Yet, the calculations by Berger *et al.* reveal that the diamond pattern might well be overridden by tilted stripes, a possibility which could be settled only by considering the long-time, fully nonlinear, regime of growth.

In the present paper, we numerically investigate the long-time dynamics of a biaxially stressed semi-infinite solid in equilibrium with its melt (or its vapor), using a phase-field model.

In recent years, this class of models has become increasingly successful in simulating realistic microstructure formation during phase transitions and materials processing. These models, which replace mathematically sharp interfaces by diffuse ones, translate into powerful numerical implementations which avoid the tracking of the interface (free-boundary problem). They are based upon a phase field ϕ which takes fixed values in bulk phases and changes smoothly from one value to another across an interfacial region. This has the advantage of regularizing unphysical singularities such as the interfacial cusps appearing in finite time in the sharp-interface models of Grinfeld instability [5,6]. The phase-field idea can be traced back to studies of phase transitions by Ginzburg and Landau [7], but it has received renewed interest because the combination of increasing computer performances and recent phase-field models make *quantitative* numerical simulations possible [8]. However, such quantitative simulations require the coupling of the phase field with other physical fields such as temperature, composition or strain. Since these fields evolve on time scales which may differ by orders of magnitude, their incorporation into the models often lead to untractable computational costs, particularly in 3D simulations. One can, by a clever adjustment of the model [9,10], suppress this limitation in the case of diffusion-controlled phase transformations such as the solidification of binary alloys at low undercooling. In the case of a phase field coupled to elastic strain variables, no trick is known. As pointed out in [11], the perturbative solution used by Müller and Grant [12] may not be fully consistent when other terms, such as gravity, are present. To go into the nonlinear regime, we choose the path of algorithmic efficiency and implement the "multigrid" algorithm [13,14] for solving the elliptic system of Lamé equations. The displacement variables are thus obtained in $O(N)$ floating points operations, the minimal algorithmic complexity achievable for fields discretized over N grid points. This efficiency allows us to explore the late stages of the full 3D Grinfeld instability.

In the present study, we use a phase-field model proposed by Kassner *et al.* [11]. It is based on the following Ginzburg-Landau free energy functional, depending on a scalar order parameter ("phase field") $\phi(\mathbf{x},t)$ coupled to an elastic strain tensor field $u_{ij}(\mathbf{x})$:

$$\mathcal{F}=\int_{\Omega}\left[\frac{1}{2}\Gamma\varepsilon^2|\nabla\phi|^2+f(\phi,u_{ij},z)\right]dV, \tag{1}$$

where the integration is performed over the entire spatial domain Ω. In Eq. (1), ε denotes the interface thickness, Γ is a reference energy density and $f(\phi,u_{ij})$ is the bulk free-

*Electronic address: jerome.paret@l2mp.fr

energy density, sum of a double-well contribution $f_{dw}(\phi)$, a gravity contribution $f_{grav}(\phi,z)$, an elastic contribution $f_{el}(\phi,u_{ij})$ and an offset contribution $f_c(\phi)$ allowing to numerically keep the equilibrium surface at a fixed altitude ζ_0. The latter contribution does not originate from a genuine physical effect. It is a modelisation trick aimed at removing the constant velocity drift experienced by a flat interface between a liquid and a solid submitted to a biaxial stress. This allows to keep the interface within the simulation box for long times. Since we only consider, in the present study, the case of semi-infinite solid, such an offset amounts to a galilean transformation leaving invariant the physics of the problem. If the presence of a substrate below the solid and its interaction with the interface had to be considered, such a corrective term would have to be avoided.

For the double-well contribution, we set $f_{dw}(\phi)=2\Gamma g(\phi)$, $g(\phi)=\phi^2(1-\phi)^2$ which insures the existence of two stable minima at $\phi=0$ and $\phi=1$. In the present study, we assignate the value $\phi=0$ and the subscript l to the liquid phase and the value $\phi=1$ and subscript s to the solid phase. Each phase is further characterized by its density ρ_α and elastic moduli μ_α and λ_α ($\alpha=l,s$). A constant surface free-energy density γ is associated with the solid-liquid interface. We then introduce a function $h(\phi)$ such that $h(0)=0$ and $h(1)=1$ in order to distinguish between each bulk phases. It allows to define continuously varying bulk physical parameters $p(\phi)=p_l+h(\phi)\Delta p$, where $p=\rho$, μ or λ and $\Delta p=p_s-p_l$. With these conventions, we put $f_{grav}(\phi,z)=\rho(\phi)g(z-\zeta_0)$ for the gravity contribution, $f_{el}(\phi,u_{ij})=\mu(\phi)u_{ij}u_{ij}+\lambda(\phi)u_{kk}^2$ for the elastic energy density and $f_c(\phi)=-h(\phi)\Sigma^2$ for the offset contribution in which Σ is a reference stress to be explicited later on [17]. Each of these contribution linearly depends on the value of the function h. Our choice for the latter function is different from the one used in [11]. We put $h(\phi)=6\phi^5-15\phi^4+10\phi^3$. This ensures that the bulk values $\phi=0$ and $\phi=1$ correspond to minima of the free energy and not only to stationary points. This enhances numerical stability for large stresses.

The field equations are obtained by a variational procedure. For a melting-crystallization phase transformation, the phase field ϕ amounts to a nonconserved order parameter and we impose upon it relaxational dynamics:

$$\frac{\partial\phi}{\partial t}=-R\frac{\delta\mathcal{F}}{\delta\phi}. \tag{2}$$

Following Kassner *et al.* [11], we set $R=1/(3k\rho_s\varepsilon)$ and $\Gamma=3\gamma/\varepsilon$ [18], where k is a rate constant with the dimension of a velocity. We obtain

$$\frac{k\rho_s}{\gamma}\frac{\partial\phi}{\partial t}=\nabla^2\phi-\frac{1}{\varepsilon^2}\left\{2g'(\phi)+\frac{\varepsilon}{3\gamma}h'(\phi)[\mu_s u_{ij}u_{ij}+\Delta\lambda u_{kk}^2+\Delta\rho g(z-\zeta_0)-\Sigma^2]\right\},$$

where primes denote derivatives with respect to ϕ [19].

Since we deal with an elastic solid, it is safe to assume that strain fields equilibrate much faster than the phase field (i.e., interfacial velocities are much smaller than sound speed). Thus they should correspond to stationary points of the free-energy functional $\mathcal{F}$:

$$\partial_j\left[\frac{\delta\mathcal{F}}{\delta u_{ij}}\right]=0. \tag{3}$$

This translates into the following system of equations:

$$\partial_j[\mu(\phi)(\partial_j u_i+\partial_i u_j)]+\partial_i[\lambda(\phi)\partial_j u_j]=0. \tag{4}$$

We have checked that, as in [11], the sharp interface limit $\varepsilon\to 0$ yields the correct expression for the velocity of the interface:

$$v_n=-\frac{1}{k\rho_s}\left\{\frac{1-\nu^2}{2E_s}(\sigma_{tt}-\sigma_{nn})^2+\gamma\kappa+\Delta\rho g(\zeta(x)-\zeta_0)-\Sigma^2\right\}, \tag{5}$$

where E_s is the solid's Young modulus and ν its Poisson ratio. σ_{tt} and σ_{nn} are respectively the tangential and normal stresses in the solid at the interface (shear components vanish by continuity of tractions across the interface). κ is the interface curvature and $\zeta(\mathbf{x})$ is the altitude of the interface at position $\mathbf{x}$. For simplicity, Eq. (5) has been written for the two-dimensional plane strain situation only. It aims at showing that the driving force for the phase transformation and for the Grinfeld instability lies in the deviation from isotropic stress. It also clarifies the way the stress parameter Σ is fixed. In order to keep a flat interface ($\kappa=0$) fixed at the altitude $z=\zeta_0$, it is immediately seen that one need to impose $\Sigma^2=[(1-\nu^2)/2E_s]\sigma_0^2$ where σ_0 is the deviatoric component of the externally applied stress.

Before going into numerical implementation of the model, one needs to specify the parameters to be used. In order to allow for a comparison, we have chosen the same convention as in [11] and set the parameters to the values of solid He, for which the Grinfeld instability has been experimentally demonstrated by Torii and Balibar [15]. These are $\rho_s=0.193$ g/cm^3, $\rho_l=0.170$ g/cm^3, $\gamma=0.2$ dynes/cm, k

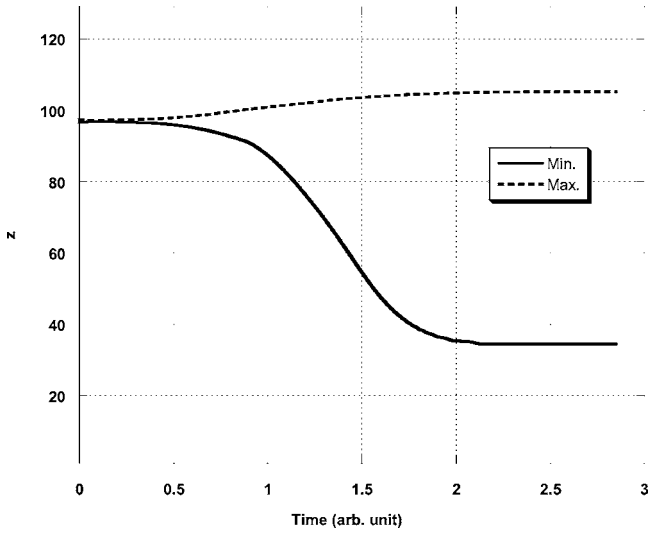

FIG. 1. Time evolution of the highest (dotted line) and lowest (thick line) points on the interface. $\sigma_{0Y}=-\sigma_{0X}=-\sigma_0$. $\sigma_0/\sigma_c=1.27$.

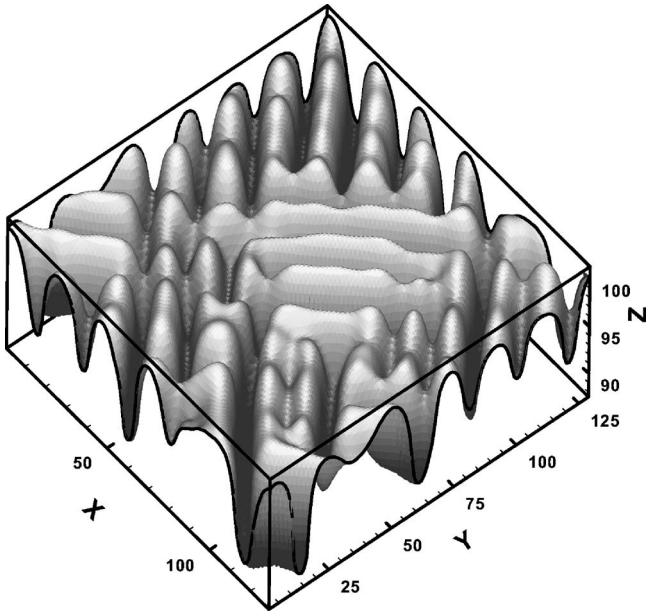

FIG. 2. Typical surface microstructure during grooving. $\sigma_{0Y}=-\sigma_{0X}=-\sigma_0$. $\sigma_0/\sigma_c=1.27$. Coordinates along the vertical axis are magnified.

$=100$ cm/s, $E=3\times10^8$ dynes/cm^2, and $\nu=0.333$ [20]. Since, aside from the pattern selection mechanism, we were interested in the saturation of the Grinfeld instability at long times, which is achieved due to the influence of gravity [11], we used the gravity constant g as a tunable parameter. The last physical parameters to be introduced are the applied stresses σ_{0X} and σ_{0Y} normal to the x and y directions respectively. For the simulations of the purely deviatoric mode $\sigma_{0X}=-\sigma_{0Y}$, we used $\sigma_{0X}=\sigma_0=6\times10^4$ dynes/cm^2. The other runs were performed at stresses such that $(|\sigma_{0X}|+|\sigma_{0Y}|)/2=\sigma_0$. These numerical parameters correspond to a Griffith length $l_G=\gamma E/\sigma_0^2$ of the order of a tenth of a millimeter and to a simulation box of the order of the millimeter. In the following, we have chosen to label all figures in number of grid points. Finally, we will label σ_c the critical stress below which the interface is stable. For the purely deviatoric mode, σ_c is given by $\sigma_c^4=(\Delta\rho g\gamma E^2)/(1+\nu)^2$.

For numerical implementation, the phase field and displacement vector field are discretized over a $128\times128\times128$ grid. The numerical procedure then consists, given the strain fields computed at the previous time step, in updating the phase field by a first order explicit Euler's scheme. The Lamé equations (4) are then solved using a multigrid algorithm. For an introduction to this class of solvers, we refer the interested reader to [14,16]. Details of the specific implementation we used will be given in a further publication. Briefly, it uses line Gauss-Seidel as a smoother, and a combination of straight injection and half-weighting for the coarse grid approximation. A comparison with a code using successive over-relaxation (SOR) was performed on a 2D 256×256 test problem and, already at this modest system size, a two orders of magnitude difference in simulation time was observed.

The simulation is initialized by filling the bottom three-quarters of the box with solid ($\phi=1$) and the top quarter with fluid ($\phi=0$). We superimpose on this planar interface a random perturbation made of the superposition of Fourier

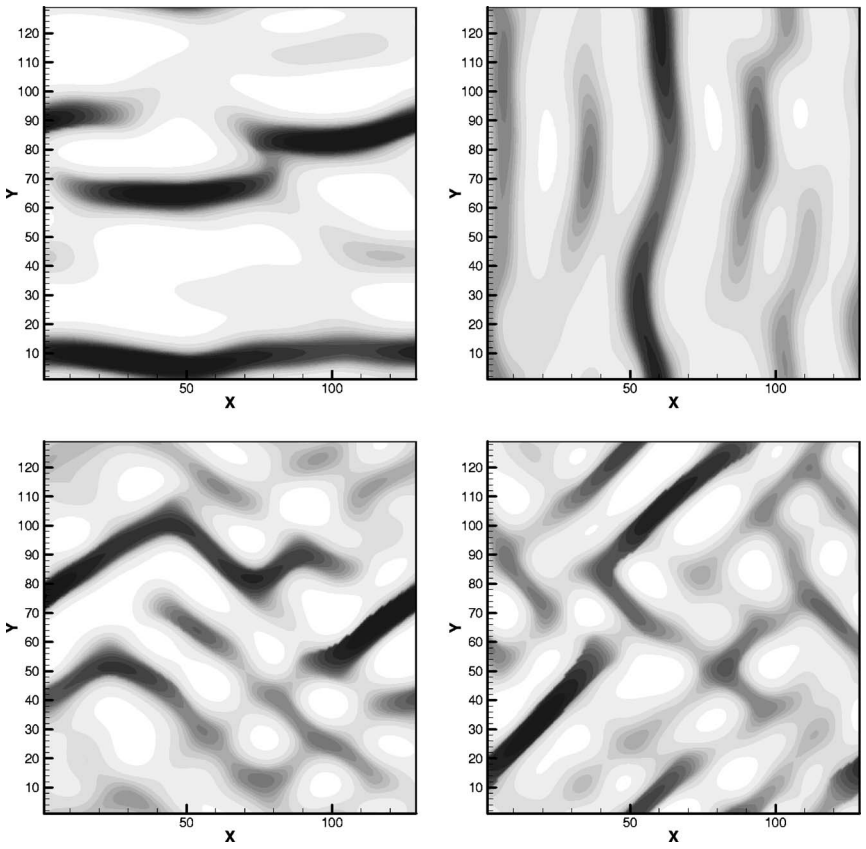

FIG. 3. Contour map of the surface during coarsening for different values of the applied stresses, without gravity ($g=0$). From top left to bottom right: I_Y, I_X, II ($\theta_\star=\pi/3$), and II ($\theta_\star=\pi/4$). Stability domains named as in [1]. Black: grooves. White: mounds.

modes with equal amplitudes and random phases. Fixed boundary conditions are imposed on the upper and lower faces, and periodic boundary conditions are imposed on the lateral faces of the cube. The latter are submitted to normal stresses, σ_{0X} and σ_{0Y} for the faces perpendicular to the x axis and y axis, respectively. We set $\varepsilon/h=2$, where h is the mesh size. The simulation are performed on a single-processor workstation and last for 1 up to 15 days, depending on the distance from the stability threshold (the closer to the threshold, the slower the evolution).

A typical time evolution of the highest and lowest points on the interface is displayed in Fig. 1. The highest points slowly grows toward a constant value, while the deepest groove evolve at a constant rate before reaching the final stationary state. The final amplitude of the microstructure depends on the value of the gravity g. The lower g, the higher the ratio σ_0/σ_c and the deeper the grooves. This evolution clearly separates into two regimes: a "grooving" regime during which "valleys" deepen at an approximately constant velocity and a final steady state regime during which no further evolution is observed. A typical structure of the surface during the grooving regime is displayed in Fig. 2.

It can be seen that this microstructure consists in striped domains with different orientations competing with each other. This is an indication that stripes with different orientations do coexist, as predicted. In order to quantitatively check those predictions, we have performed simulations with different applied stresses, corresponding to different regions of the phase diagram established by Berger *et al.* [1]. There are 3 different sectors: sectors I_X and I_Y correspond respectively to stripes parallel to the y and x axis, sector II corresponds to stripes with inclination $\pm\theta_\star$ as given by

$$\cos 2\theta_\star = \frac{(1-\nu)(\sigma_{0Y}+\sigma_{0X})}{\nu(\sigma_{0X}-\sigma_{0Y})}, \tag{6}$$

where ν is the Poisson ratio of the solid. In sector II, we have chosen external stresses so as to obtain $\theta_\star=\pi/3$ and $\theta_\star=\pi/4$. The results are displayed in Fig. 3, which shows contour maps of the surface during the grooving regime. Although the observed stripes are still distorted at this stage of the simulation, it is seen that the predicted orientations are correct.

However, from the numerical results, it appears that the "diamond morphology" terminology is misleading. Stripes with different orientations are observed at different spatial positions and tend to form domains with a well-defined tilt angle. This is coherent with the physical space picture of Grinfeld instability consisting in a competition of grooves, the deepest ones screening the others and making them recede. Indeed, in our simulations, a single orientation always wins, as suggested by the weakly nonlinear analysis of [1]. We typically observe one single groove as a final state. Such a stationary groove is displayed in Fig. 4. Note that, since horizontal boundary conditions are periodic, the observed two grooves are indeed portions of a single one.

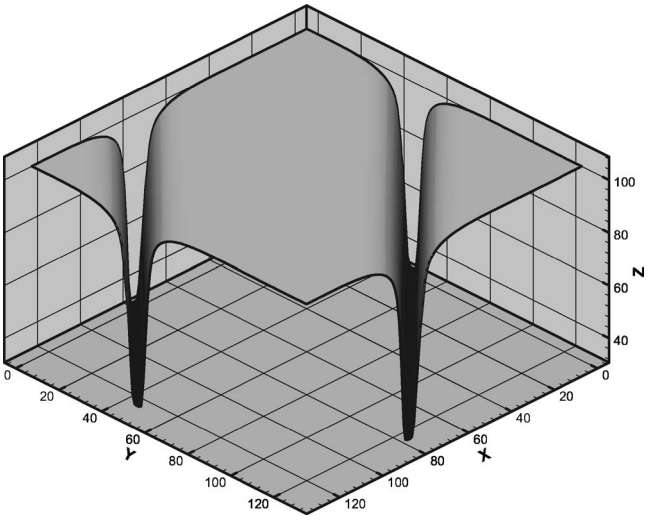

FIG. 4. Stationary state of a biaxially stressed surface. $\sigma_{0Y}=-\sigma_{0X}=-\sigma_0$; $\theta_\star=\pi/4$. $\sigma_0/\sigma_c=1.27$.

Because our simulations are fully nonlinear, we can go further than the weakly nonlinear regime and achieve the saturation of the instability. It appears that the answer to the question "does the striped pattern override the diamond morphology before saturation?" is "yes." Even in the case where saturation is achieved at a low groove amplitude [Fig. 5 (left)], near to the stability threshold ($\sigma_0/\sigma_c=1.01$), a single orientation is obtained.

These observations raise the question of the existence of a "quantum dots" regime in the present model. Although "diamond" patterns appear to be absent, one sould notice that purely biaxial stress ($\sigma_{0Y}\neq\sigma_{0X}$) is not necessarily the most interesting situation. The degenerate case of isotropic biaxial stress ($\sigma_{0Y}=\sigma_{0X}$), which corresponds to a critical line in the phase diagram presented in [1], proves to have a rich behav-

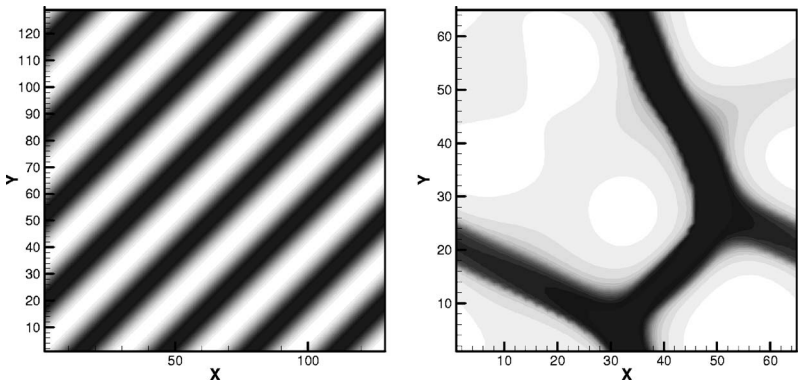

FIG. 5. Left: Final state with parallel stripes. $\sigma_{0Y}=-\sigma_{0X}=-\sigma_0$. $\sigma_0/\sigma_c=1.01$. Right: A particular final state obtained with isotropic biaxial stress $\sigma_{0Y}=\sigma_{0X}$. Horizontal boundary conditions being periodic, repetition of the computation box yields a hexagonal pattern. $64\times64\times64$ grid.

ior, yielding nontrivial patterns. As an example, we show in Fig. 5 (right) how 3 different orientations can lock into an hexagonal pattern, a periodic array of "dots" separated by deep trenches.

This is certainly not all of the story. Indeed, the present model is a rather crude one. While it is quite useful, owing to its simplicity, for assessing on a fundamental level the long-time behavior of the Grinfeld instability, it would need to be extended in order for it to capture the physics of quantum dots formation on a solid substrate. Two extensions, which are currently under implementation, sound crucial to us: the introduction of the substrate into the model and that of crystalline anisotropy which effects on the surface free energy are known to strongly influence morphologies in almost any growth phenomenon.

In summary, we have performed the first 3D numerical simulations of the biaxial Grinfeld instability using a phase-field model. The nontrivial question of pattern selection for biaxial stresses, specially the case of one compressive and one tensile principal stresses, has been settled in the case of isotropic materials. The predictions of Berger *et al.* [1] have been confirmed and extended to the fully nonlinear regime which is presently outside the reach of analytical calculations and of sharp-interface approaches. The phase-field framework of the present model could be easily extended to more complex situations, particularly the ones relevant to the physics of thin films and quantum dots growth. The combined efficiency of the phase-field technique and of the multigrid algorithm provides a powerful tool to investigate the latter situations.

Professor K. Kassner is gratefully acknowledged for many stimulating discussions and for providing numerical data obtained with SOR to compare with the multigrid algorithm.

[1] P. Berger, P. Kohlert, K. Kassner, and C. Misbah, Phys. Rev. Lett. **90**, 176103 (2003).
[2] R. Asaro and W. Tiller, Metall. Trans. **3**, 1789 (1972).
[3] M. Grinfeld, Sov. Phys. Dokl. **31**, 831 (1986).
[4] Y. W. Zhang and A. F. Bower, J. Mech. Phys. Solids **47**, 2273 (1999).
[5] C. H. Chiu and H. Gao, Int. J. Solids Struct. **30**, 2983 (1993).
[6] B. J. Spencer and D. I. Meiron, Acta Metall. **42**, 3629 (1994).
[7] V. Ginzburg and L. D. Landau, JETP **20**, 1064 (1950).
[8] J. C. Ramirez, C. Beckermann, A. Karma, and H. J. Diepers, Phys. Rev. E **69**, 051607 (2004).
[9] A. Karma and W. J. Rappel, Phys. Rev. E **57**, 4323 (1998).
[10] A. Karma, Phys. Rev. Lett. **87**, 115701 (2001).
[11] K. Kassner, C. Misbah, J. Müller, J. Kappey, and P. Kohlert, Phys. Rev. E **63**, 036117 (2001).
[12] J. Müller and M. Grant, Phys. Rev. Lett. **82**, 1736 (1999).
[13] A. Brandt, Math. Comput. **31**, 333 (1977).
[14] W. H. Press, S. A. Teukolsky, W. T. Vetterling, and B. P. Flannery, *Numerical Recipes in C–Second Edition* (Cambridge University Press, Cambridge, England, 1992).
[15] R. H. Torii and S. Balibar, J. Low Temp. Phys. **89**, 391 (1992).
[16] P. Wesseling, *An Introduction to Multigrid Methods* (John Wiley and Sons, New York, 1991).
[17] In order to simplify the above formulas, we chose as a reference state for strain an equilibrium state with zero stress. Although we stick to this prescription in the present paper, the problem of reference state specification should not be overlooked as it may be important in the case of prestrained bodies (see [11] for a discussion).
[18] It is the analysis of the sharp interface limit, i.e., the limit $\varepsilon/l_c \to 0$ (l_c a characteristic length of the problem) which dictates the relation between model parameters Γ, R and physical parameters γ, k, ρ_s.
[19] Since we consider the phase $\phi=0$ to be a liquid, its shear modulus μ_l vanishes. Thus $\Delta\mu=\mu_s$.
[20] The conversion from the parameters E, ν to the moduli μ, λ is standard and found in any textbook on elasticity.